Applied Ecology and Environmental Sciences, 2023, Vol. 11, No. 2, 42-53
Available online at http://pubs.sciepub.com/aees/11/2/1
Published by Science and Education Publishing
DOI:10.12691/aees-11-2-1

Impregnated Activated Carbon Made from Buffalo Dung: Electrical and Photoluminescence Investigations

Suher M Dawoud, Mouayed A Hussein*, Raed K Zaidan

Department of Chemistry, College of Science, University of Basrah, Iraq
*Corresponding author: mouayed_505emar@yahoo.com

Received February 07, 2023; Revised March 14, 2023; Accepted March 27, 2023

Abstract Activated carbon was made from buffalo dung. The carbon was activated by KOH that of char: KOH: H_2O is 3:4:5. The obtained AC was modified with 5% of Selenium, Bismuth and zirconium. For the obtained samples, the nitrogen adsorption- desorption isotherm, surface area, total volume, micro volume and the mean pore diameter were characterized by Brunauer Emmett Teller (BET), the pore size distribution was characterized by Barrett Joyner Halenda (BJH), the surface morphology was characterized by scanning electron microscopy (SEM), the elemental composition was characterized by energy dispersive X-Ray spectroscopy (EDX), and the crystallographic structure was characterized by X-rays Diffraction (XRD). The obtained results have been revealed higher amount of pores in mesoporous region (2-50 nm) and few pores in microporous region (> 2 nm). The XRD and SEM showed the crystallinity of modified ACs is increased compare to the ACs. The EDX showed successfully modification of ACs with Se, Bi and Zr. The electrical properties of the samples were investigated by four point probe method. The resistance (R), standard resistivity (ρ_0) and conductivity (σ) were extracted. Moreover, the galvanostatic charge discharge profiles of the samples were also investigated. The obtained results exhibited that small amount quantity of charge (Q) passes through AC compared to its modified peers. The quantum dot technology was used to investigate the optical property of AC. The method was accomplished by UV-Vis absorption and fluorescence emission. The UV–Vis spectrum showed an absorption band at 275 nm and the fluorescence emission shows a green photoluminescence emission at 480 nm. The obtained photoluminescence property reveals it may be useful as an accurate nanotechnology for cancer detection and energy-transfer compound in photocatalytic applications.

Keywords: *activated carbon, 4-point probe, resistivity, quantum dot, photoluminescence*

Cite This Article: Suher M Dawoud, Mouayed A Hussein, and Raed K Zaidan, "Impregnated Activated Carbon Made from Buffalo Dung: Electrical and Photoluminescence Investigations." *Applied Ecology and Environmental Sciences*, vol. 11, no. 2 (2023): 42-53. doi: 10.12691/aees-11-2-1.

1. Introduction

Due to their cheapness and availability, the carbon materials are ideal targets to be used in a wide range of applications depending on their electrical conductivity, polarizability, chemical inertness and structural strength along with tunable electrical, thermal and optical properties [1,2]. Porous carbon materials are very popular as electrode materials for lithium secondary battery, supercapacitor, dye sensitized solar cell and fuel cell [3,4,5,6]. Porous carbon materials can be characterized into three types based on their pore sizes: microporous < 2 nm, 2 nm < mesoporous < 50 nm and macroporous > 50 nm. Many methods have been developed for synthesis the porous carbon materials as for examples, hard or soft sacrificial template using silica or surfactant, catalytic activation using metal salts or organometallic compounds, carbonization of polymer blends and aerogel, chemical activation, and physical activation [7,8,9,10]. Development of simple low-cost methods is still a premier challenge for synthesis of nanostructured carbon materials [11].

Biomass waste such as pine needles, corn stalk, coffee bean, rice straw and cow dung has known as a new precursor for the production of carbon-based materials due to its carbon richness, low cost, ease to access, ubiquitous, renewable and environmental-friendliness [12,13,14,15].

Carbon quantum dots (CQDs) have been reported in 2004 while separating single walled carbon nanotubes by engraving electrophoresis [16]. It has been noticed that CQDs with novel optical properties, outstanding biocompatibility and robust chemical inertness are of potent probes in high contrast bioimaging and biosensing, and that CQDs with potent photoluminescence are of particular importance in catalysis and fields of energy. According to these findings, the interest to develop novel methods becomes necessary to make high quality CQDs with tuned properties in high yield. Different carbon

precursors including graphite [17,18,19], graphene oxides [20], fullerene [21], carbon fibers [22] and organic carbon sources [23,24,25], have been used to prepare CQDs. Most of carbon precursors are relatively expensive, which results in a high preparation cost of CQDs to some degree.

Buffalo dung is a renewable resource because it mainly comes from the undigested residue of cellulose based feeds being excreted by this animal. Generally, buffalo dung was converted into fertilizer or soil amendment by composting because composted manure contains many dissolved organic matter fractions [26]. Without proper treatment or management, it can cause some environmental problems, including air quality deterioration, public hazards of infectious pathogen and asphyxia poisoning, greenhouse gas emissions of carbon dioxide and methane, and water pollution [27]. Due to its high carbon content, this biomass resource can be thermally converted into biochar used as an adsorbent [28,29,30].

Buffalo breeding is widely spread in rural areas of southern Iraq, especially in marshlands. It represents the main source for survival of local people in marshlands. Buffalo dung has been used for centuries as cooking fuel, sanitizing cleanser, construction material, insulation, and water proofing for walls and floors in rural houses.

In this study, we have synthesized activated carbon from buffalo dung, a cheap and abundant biological waste, by using KOH as activating agent. The obtained activated buffalo dung carbon is modified with metals of Selenium, Bismuth and Zirconium. The electric properties of activated carbon and its modified peers and photoluminescence property of synthesized activated carbon are investigated.

2. Material and Methods

2.1. Preparation of Activated Carbon

Buffalo dung (BD) was collected from the rural area of Karmat-ali, north of Basrah province. The BD mass was wash and dried under the sunlight, burning at a temperature of (450)°C for 2h. The resulting char then activated by mixing with potassium hydroxide at ratio of char: KOH: H_2O of 3:4:5, the mixture leaves on continuous stirring at 80°C until a homogeneous product is formed. The product then transferred to ceramic crucible and calcined in oven by raising the temperature by 10 degrees per minute up to 550°C for 2 hr, then the product leaves to cool inside the oven, then washed with 0.1 M HCl to removes the impurities, then washed with deionized water until the washing water becomes neutral and finally the product is dried at 80°C for 24 hr. The obtained activated carbon is assigned as F1.

2.2. Modification of F1 with Selenium, Bismuth and Zirconium

The activated carbon (AC) is modified with Selenium, Bismuth and Zirconium. 1 g of AC and 5% for each of SeO_3, Bi_2O_3 or $ZrCl_4$ was suspended in a mixture of ethanol: water (1:4), the suspension was left for 2hr under stirring at 70°C, then filtrated, washed several times with water and dried at 120°C for 24 hr. The obtained carbons modified Se, Bi and Zr are assigned F1Se, F1Bi and F1Zr.

2.3. Electrical Testing Method of F1 and It's Modified Peers

Electrical testing of F and it's modified peers of F1Se, F1Bi and F1Zr was investigated by four point probe method. The samples were annealed with the Poly(methyl methacrylate) (PMMA), that is a lightweight insulating polymer has possesses good dimensional and mechanical stability to form unique material systems. PMMA pellets were dried at 60°C in a vacuum oven for 24 h. The PMMA pellets were first dissolved into solution with chloroform and then mixed with amounts of samples and expanded in a template. The solvent was evaporated at 60 0C and the blends were dried at the same temperature in a vacuum oven for 24 h. The composites then submitted to the 4-point probe experiment. Four collinear and equidistant probes are placed on the surface of sample, outer probes are connected to current and the inner probes supply for the measurement of voltage.

2.4. Synthesis of Quantum Dot (CD)

25 mL of concentrated HNO_3 and $HClO_4$ at a molar ratio of 1:1 was mixed with 1.00 g of F1 that crushed carefully in a 100 mL round-bottom flask. Oxidation was carried out under microwave radiation heating (500 W) at 100°C for 120 min. After cooling, the black suspension was neutralized with ammonium hydroxide to pH 7.0 and then separated using a 1000 Da ultrafiltration membrane in an MSC300 ultrafiltration device. The filtrate was concentrated in vacuum and then dialyzed with a molecular weight cut-off of 300 for 3 days to remove the inorganic ions. Finally, pure CQD were obtained and denoted as 550-CQD [31].

2.5. Characterization

The F1 and it's modified peers were characterized by FTIR, Brunauer Emmett Teller (BET), Barrett Joyner Halenda (BJH), X-rays Diffraction (XRD), Scanning Electron Microscopy (SEM) and Energy Dispersive X-Ray Spectroscopy (EDX). The electrical testing was carried out using 4-poind probe technique, and the quantum dot was investigated by UV-Visible spectroscopy, and the photoluminescence was investigated by fluorescence emission spectroscopy.

3. Results and Discussion

3.1. Characterization of F1

3.1.1. FTIR Spectroscopy Analysis

FTIR analysis was used for identifying surface functional groups of the activated carbon. Figure 1 is represent the FT-IR spectrum of prepared activated carbon (F1) at 550°C. The broad peak around 3441 cm^{-1} is associated to the bands of O–H group. The peak at 2899 cm^{-1} is attributed to presence of aliphatic C–H stretch of CH, CH_2 and CH_3 groups. The peak which is presented at 1637 cm^{-1} can be corresponded to C=O stretching of carboxylic acids. The band 1444 cm^{-1} assigns to C-H asymmetric and symmetric bending vibrations. The band in the range between 1085 cm^{-1} may be due to the presence of C–O group. The band found at 794 cm^{-1} is related to the stretching vibrations of C−H out-of-plane band [32,33].

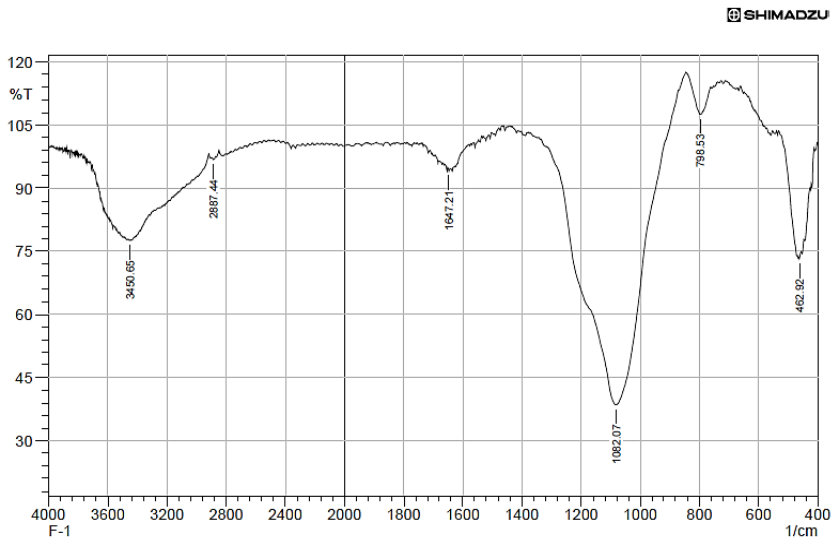

Figure 1. FTIR spectrum of F1

3.1.2. Surface Area and Pore Structure

The BET Equation 1 uses the information from the isotherm to determine the surface area of the sample, where *X* is the weight of nitrogen adsorbed at a given relative pressure (*P/Po*), *Xm* is monolayer capacity, which is the volume of gas adsorbed at standard temperature and pressure (STP), and C is constant. STP is defined as 273 K and 1 atm.

$$\frac{1}{X_m\left[\left(\frac{p}{p_0}\right)-1\right]}=\frac{1}{X_mC}+\frac{C-1}{X_mC}\left(\frac{p}{p_0}\right) \quad (1)$$

The plot $\frac{\frac{P}{P_0}}{X_m(1-\frac{P}{P_0})}$ versus $\frac{P}{P_0}$ gives a linear region can usually be found. The slope and intercept of this line can then be used to calculate *Xm*, the amount adsorbed at the statistical monolayer, as well as *C*, the BET constant.

Once *Xm* is determined, the total surface area *S* can be calculated with the following equations 2 and 3 where *Lav* is Avogadro's number, A_m is the cross sectional area of the adsorbate and equals 0.162 nm^2 for an absorbed nitrogen molecule, and *Mv* is the molar volume and equals 22.414 L.

$$X_m=\frac{1}{s+i}=\frac{C-1}{C_s} \quad (2)$$

$$S=\frac{X_mL_{av}A_m}{M_v} \quad (3)$$

The adsorption-desorption isotherms of the biomass-derived activated carbons are presented in Figure 2. The profile reveals similar type II isotherm which is characteristic of high amount of mesopore volume with microporous materials. The BET isotherm indicated that has narrow micropores with sizes less than 1 nm. At higher P/P_0, larger N_2 uptakes recorded for the activated carbon, this indicates it has wider pore size and indicates that in mesoporous region. The results are further supported by the pore size distribution using Barrett-Joyner-Halenda (BJH) method, through applied to nitrogen desorption data measured at 77 K as displayed in Figure 2. The BJH pore size distribution shows higher amount of pores in mesoporous region (2-50 nm) and few pores in microporous region (1.21-1.85 nm) [34]. Table 1 displays the porosity data obtained from N_2 sorption isotherm analysis.

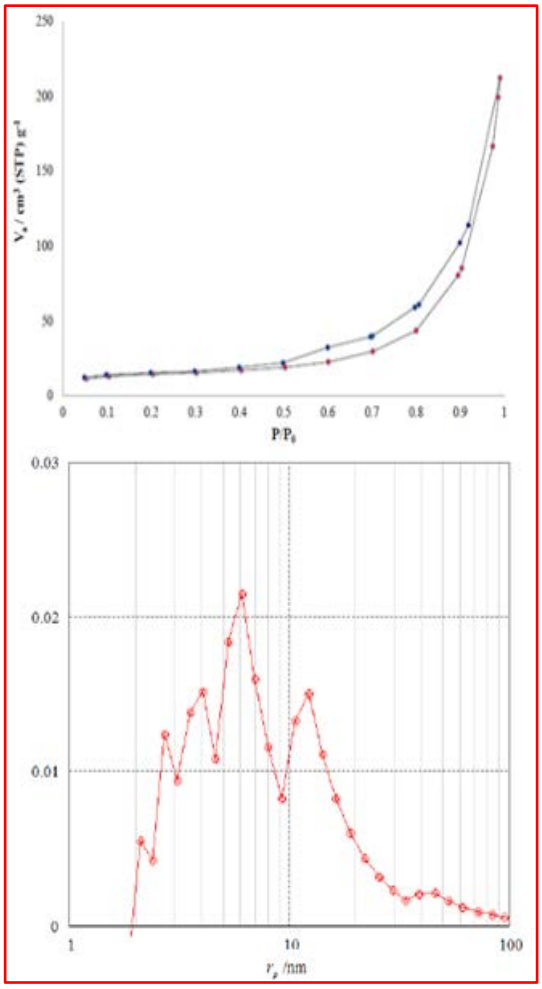

Figure 2. (Up) Nitrogen adsorption-desorption isotherm and (Down) pore size distribution obtained from BJH method of F1

Table 1. Porosity parameters of AC obtained from BET analysis

Parameter	F1
S_{BET} (m^2g^{-1})	103.24
V_{Total} (cm^3 g^{-1})	0.6542
Vm (cm^3(STP) g^{-1})	23.719
Mean pore diameter (nm)	25.349

3.1.3. X-ray Diffraction (XRD) Analysis

The crystallography and crystallinity of F1 is analyzed via XRD and presented in Figure 3. The XRD patterns exhibited complete carbonization by showing an amorphous structure and shown two major diffraction broad peaks at 26° and 43°. These two peaks are the confirmation of the plane (002) and (101) for carbon materials respectively. Diffraction peaks around 26° were the indication of the fragmented devolved crystallite aromatic structure and a broad and weak peak at 43° was the indication of an amorphous structure having very little graphitization degree. The peak pattern of AC has clear accordance with previous literature findings [35].

The initial values of the size of F1 particle were calculated according to the Scherrer formula:

$$D_{hkl} = \frac{K\lambda}{\beta cos\theta} \quad (4)$$

where K is the particle shape factor, 0.9, λ is X-ray wavelength, 1.54060 Å, β is the half-width of (hkl) reflection, θ = 2θ/2 is Bragg angle corresponding to (hkl) reflection. The results are revealed that D_{hkl} is 26.24311 Å [36].

3.1.4. Surface Morphology by Scanning Electron Microscope (SEM)

The surface morphologies of the synthesized activated carbon is characterized by emission scanning electron microscopy, SEM micrograph shown in Figure 4 reveals highly irregular and rough surface stature originated from highly porous morphology can be observed. F1 show a particle size of 31.38 to 68.42 nm, with medium particle size of 42.84 nm.

3.1.5. Energy Dispersive X-ray (EDX) Analysis

The SEM results were assisted by an electron microprobe (EDX) to determine the majority components of activated carbon. The results are shown in Figure 5. Buffalo dung contains undigested remaining of cattle feed and therefore contains lots of inorganic non-volatile materials and/or thermally unstable organic impurities. Due to high temperature treatment followed by washing with 1.0M HCl solution during activation, the impurities were removed from the carbonaceous materials leaving behind abundant pores in AC samples along with pores created by KOH activation. Since chemical activation generally leads to the formation of high amount of mesopores in the carbon sample can be mainly attributed to removal of inorganic materials present in BD.

3.2. Characterization of Modified F1

3.2.1. Surface Area and Pore Structure

The adsorption-desorption isotherms of the modified F1 are presented in Figure 6. All the modified profiles reveal similar type II isotherms which are characteristic of high amount of mesopore volume with microporous materials. The F1 modified-Zr of F1Zr reveals type I isotherm which is characteristic for both micropore and mesopore volume compared to other modified profiles. The BJH pore size distribution shows amount of pores in microporous region (1-10 nm) for F1Zr addition to amount of pores in mesoporous region (2-50 nm). Table 2 displays the porosity data obtained from N_2 sorption isotherm analysis.

3.2.2. XRD Analysis

The crystallography and crystallinity of the modified samples is analyzed via XRD and presented in Figure 7. The XRD patterns exhibited that the crystallinity of the entire carbon surface increases after modification with Bi. The amorphous structure shown the major diffraction broad peak at 26° and the major broad peak at 43° appeared between 40° and 50°. The high crystallinity of carbon modified Bi shows the major diffraction peak at 26° and at 45° with additional characteristic diffraction peaks at 2θ = 30.31, 33.30, 50.04, 59.04 and 63.56°, corresponding to the reflection planes of the structure of the Bi_2O_3. The additional weak peaks observed in the diffractogram are attributed to the hydroxides of Bi present in the sample. The initial values of the size of carbon modified particles are calculated by Scherrer formula and the obtained results are listed in Table 3.

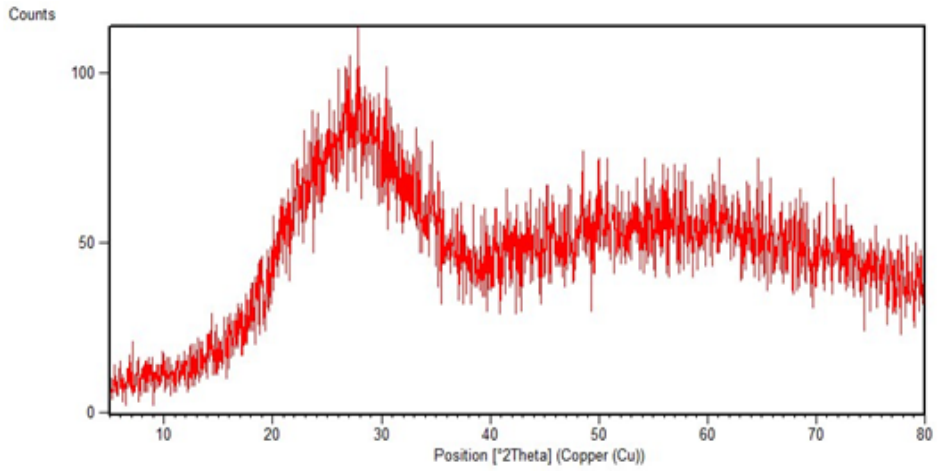

Figure 3. XRD analysis of F1

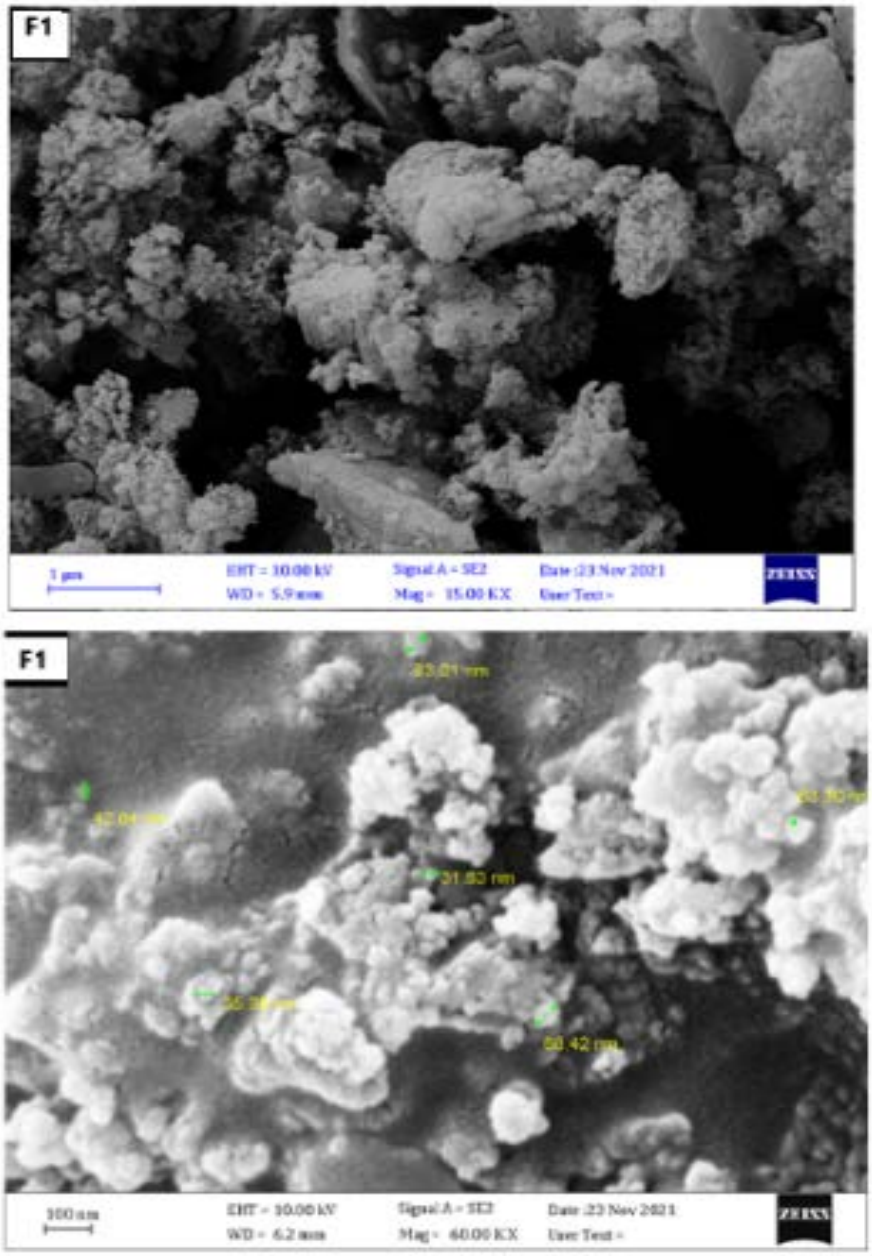

Figure 4. SEM images of F1

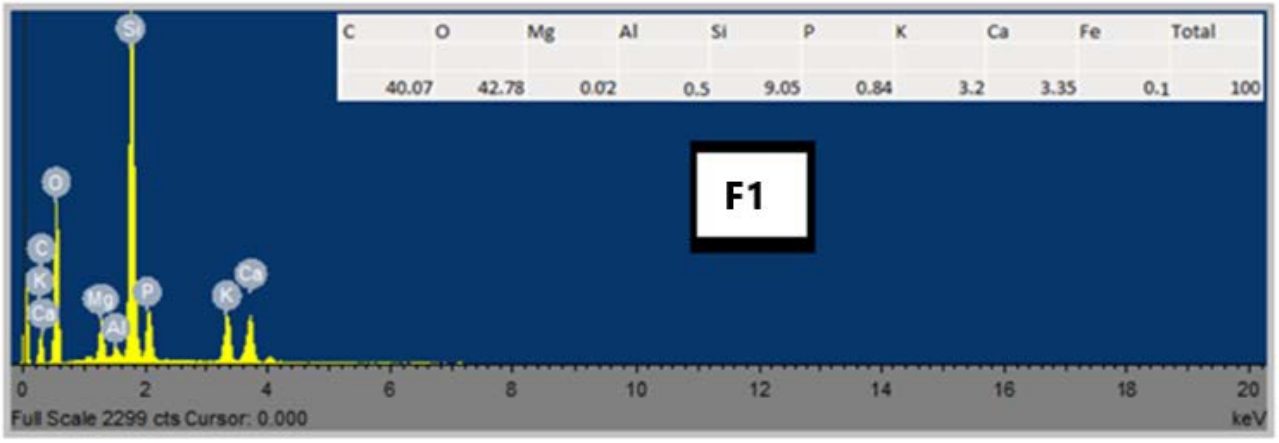

Figure 5. EDX spectra of F1

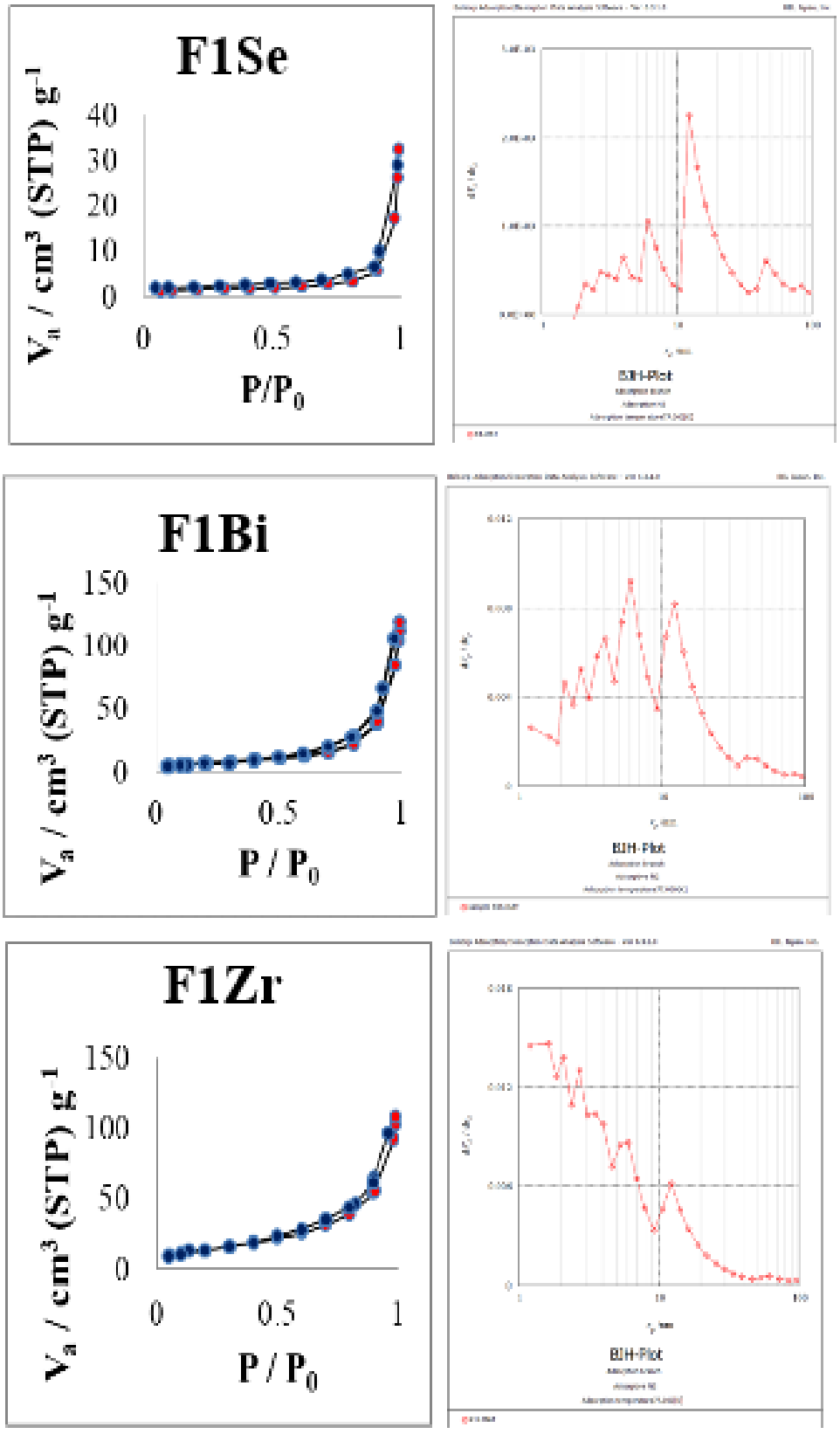

Figure 6. (Left) Nitrogen adsorption- desorption isotherm and (Right) pore size distribution obtained from BJH method of F1Se, F1Bi and F1Zr

Table 2. Porosity parameters of modified F1 obtained from BET analysis

Modified F1	S_{BET} (m^2g^{-1})	V_{Total} (cm^3 g^{-1})	V_m (cm^3(STP) g^{-1})	Mean pore diameter (nm)
F1Se	5.2598	0.046890	1.2085	35.660
F1Bi	26.789	0.1731	6.1550	25.845
F1Zr	50.319	0.1595	11.561	12.678

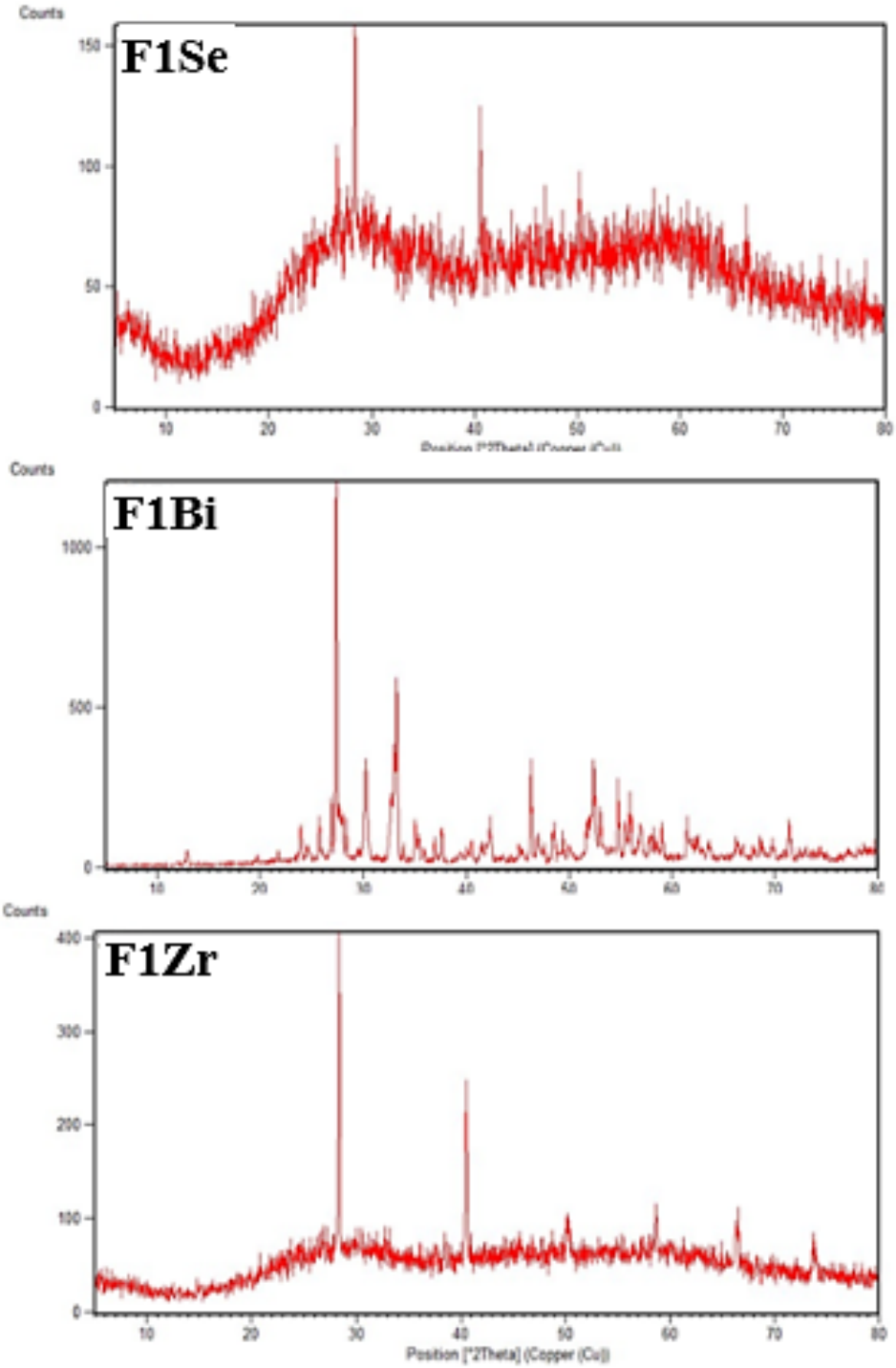

Figure 7. XRD analysis of F1Se, F1Bi and F1Zr

Table 3. The particle size values of modified carbon

Modified carbon	$D_{(hkl)}$ (Å)
F1Se	49.66432
F1Bi	50.21651
F1Zr	65.29676

3.2.3. Surface Morphology by SEM

The surface morphologies of the modified carbon were characterized by emission scanning electron microscopy. Unlike to irregular and rough surface stature that shown for AC, the SEM micrographs of modified AC shown in Figure 8 reveal highly regular surface stature. Carbon modified of F1Se and F1Bi show hollow nanotubes.

3.2.4. EDX Analysis

The modification of activated carbons was determined by an electron microprobe (EDX). The results are shown in Figure 9. Buffalo dung contains undigested remaining of cattle feed and therefore contains lots of inorganic non-volatile materials and/or thermally unstable organic impurities.

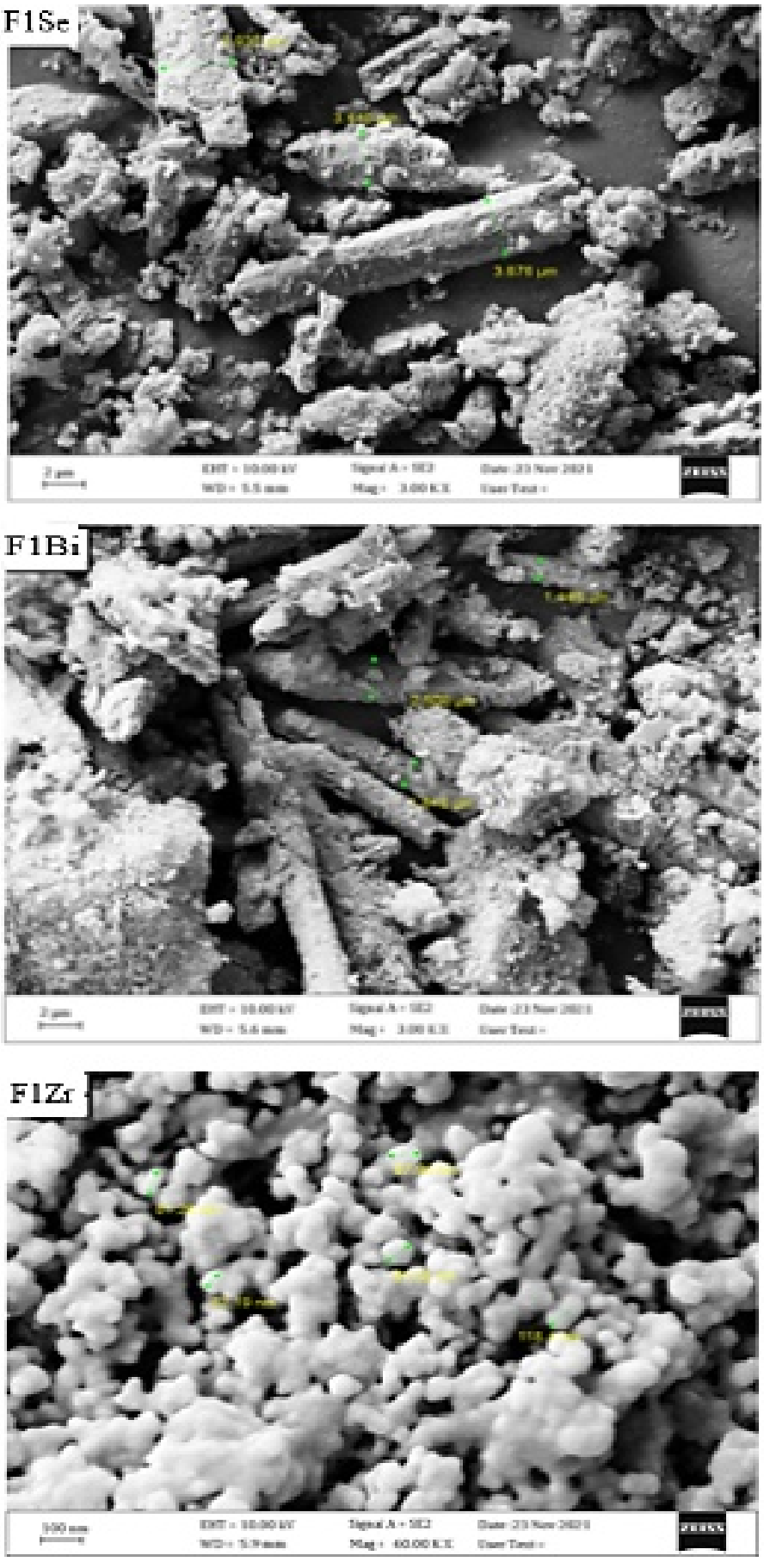

Figure 8. SEM images of F1Se, F1Bi and F1Zr

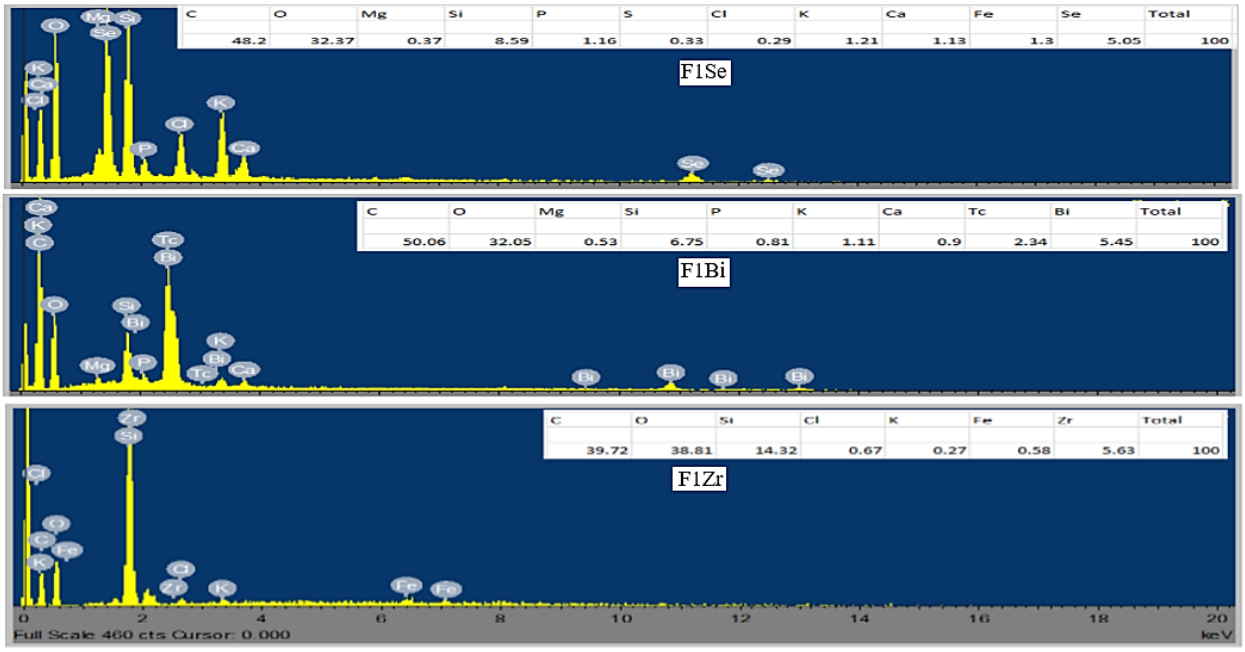

Figure 9. EDX spectra of F1Se, F1Bi and F1Zr

3.3. Electrical Testing

The templates composites of F1 and it's modified peers are shown in Figure 10. The composites are submitted to the 4-point probe experiment. Four collinear and equidistant probes are placed on the surface of sample, outer probes are connected to current and the inner probes supply for the measurement of voltage.

Figure 10. Templates of the samples for 4-point probe

The graph of current (I) versus voltage (V) shown in Figure 11 reveals that the increases the voltage leads to increases the current, this mean that the resistance decreases during this route. The resistance can be calculated by ohm's law (equation 5).

$$R = \frac{V\,(Volt)}{I\,(Amp)} \tag{5}$$

The standard resistivity (ρ_0) is calculated by the equation 6.

$$\rho_0 = R * 2\pi s \tag{6}$$

$$\sigma = \frac{1}{\rho_0} \tag{7}$$

Where, s is the spacing between point probes (2mm) and σ is the conductivity of the material. The obtained results fit to equations 5, 6 and 7 are tabulated in Table 4-Table 7 of F1, F1Se, F1Bi and F1Zr, respectively.

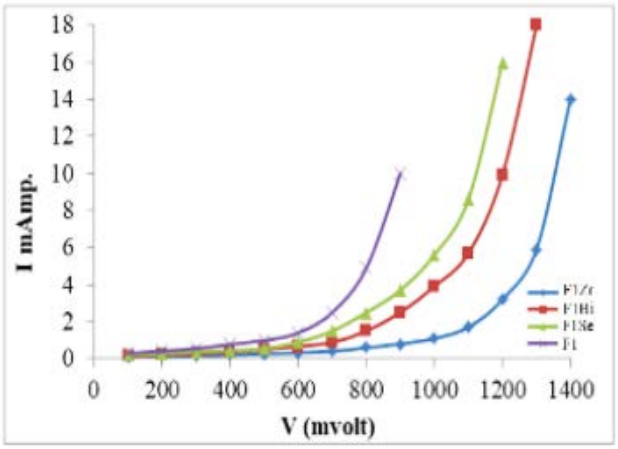

Figure 11. Graph the current vs. voltage of F1, F1Se, F1Bi and F1Zr

The data displayed that the conductivity increased after exceeded the threshold voltage and follows the order F1Bi> F1Se> F3> F1Zr. These results can be attributed to the crystallinity and the mesoporous region of samples. The more crystallinity and amount of mesopore volume leads to more conductivity and less resistivity. Meso pores can allow to facile electrons movement and thus to effectively access active surfaces present in micropores that play limited role in storing charges. F1Bi and F1Se have more amount of mesopore volume and more crystallinity than that for F1 and F1Zr which are an amorphous and small amount of mesopore volume.

Table 4. Standard resistivity (ρ_0) and Conductivity (σ) of F1

V (Volt)	I (Amp)	R (Ω)	ρ_0 (Ωm)	σ (Ω m)$^{-1}$
0.1	0.0003	333.33	4.18	0.239
0.2	0.00041	487.80	6.12	0.163
0.3	0.00056	535.71	6.72	0.148
0.4	0.00078	512.82	6.44	0.155
0.5	0.00099	505.05	6.34	0.157
0.6	0.0014	428.57	5.38	0.185
0.7	0.0025	280	3.51	0.284
0.8	0.0049	163.26	2.05	0.487
0.9	0.010	90	1.13	0.884

Table 5. Standard resistivity (ρ_0) and Conductivity (σ) of F1Se

V (Volt)	I (Amp)	R (Ω)	ρ_0 (Ωm)	σ (Ω m)$^{-1}$
0.1	0.0002	500	6.28	0.159
0.2	0.00026	769.23	9.66	0.103
0.3	0.00038	789.47	9.91	0.100
0.4	0.00044	909.09	11.41	0.087
0.5	0.00055	909.09	11.41	0.087
0.6	0.00090	666.66	8.37	0.119
0.7	0.0015	466.66	5.86	0.170
0.8	0.0025	320	4.02	0.248
0.9	0.0037	243.24	3.05	0.327
1.0	0.0056	178.57	2.24	0.446
1.1	0.0086	127.90	1.60	0.625
1.2	0.016	75	0.94	1.063

Table 6. Standard resistivity (ρ_0) and Conductivity (σ) of F1Bi

V (Volt)	I (Amp)	R (Ω)	ρ_0 (Ωm)	σ (Ω m)$^{-1}$
0.1	0.00013	769.23	9.66	0.103
0.2	0.0002	1000	12.56	0.079
0.3	0.00028	1071.42	13.45	0.074
0.4	0.00037	1081.08	13.57	0.073
0.5	0.00049	1020.40	12.81	0.078
0.6	0.00066	909.09	11.41	0.087
0.7	0.00089	786.51	9.87	0.101
0.8	0.0015	533.33	6.69	0.149
0.9	0.0025	360	4.52	0.221
1.0	0.0039	256.41	3.22	0.310
1.1	0.0057	192.98	2.42	0.413
1.2	0.0099	121.21	1.52	0.657
1.3	0.018	72.22	0.90	1.111

Table 7. Standard resistivity (ρ_0) and Conductivity (σ) of F1Zr

V (Volt)	I (Amp)	R (Ω)	ρ_0 (Ωm)	σ (Ω m)$^{-1}$
0.1	0.0001	1000	12.56	0.079
0.2	0.00015	1333.33	16.74	0.059
0.3	0.00017	1764.70	22.16	0.045
0.4	0.0002	2000	25.12	0.039
0.5	0.00025	2000	25.12	0.039
0.6	0.00032	1875	23.55	0.042
0.7	0.0004	1750	21.98	0.045
0.8	0.0006	1333.33	16.74	0.059
0.9	0.0008	1125	14.13	0.070
1.0	0.0011	909.09	11.41	0.087
1.1	0.0017	647.05	8.12	0.123
1.2	0.0032	375	4.71	0.212
1.3	0.0059	220.33	2.76	0.362
1.4	0.014	100	1.25	0.8

Figure 12 shows the typical galvanostatic charge discharge profiles of the samples. The graphs display that the charge discharge accomplish in 5, 7, 9 and 10.1 seconds for F1, F1Se, F1Bi and F1Zr, respectively. The quantity of charge (Q) can be calculated from the equation 8.

$$Q = It \tag{8}$$

At maximum current of 15, 14, 11.2 and 10.1 mA, the quantity of charge in coulomb is 0.075, 0.098, 0.1008 and 0.101 for F1, F1Se, F1Bi and F1Zr, respectively. It can be said that the metal modification improves the electrical qualities of the surface.

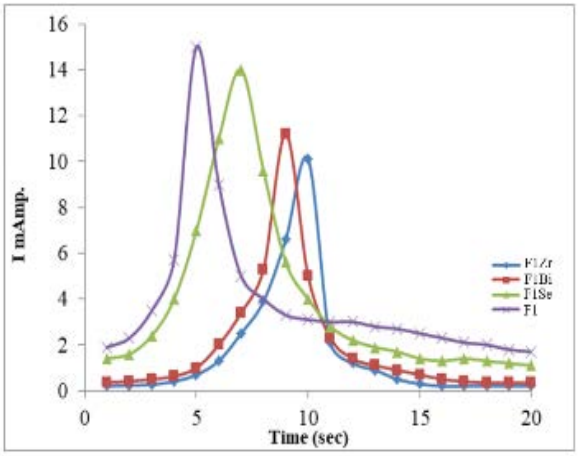

Figure 12. Galvanostatic charge-discharge profiles of F1, F1Se, F1Bi and F1Zr

3.4. Photoluminescence Property of F1

F1 quantum dot was synthesized according the procedure mentioned above, pure CQD was obtained and denoted as 550-CQD. The optical property of 550-CQD is investigated by UV–Vis absorption and fluorescence spectroscopy. Figure 13A is the UV–Vis spectrum of 550-CQD, showing an absorption band at 275 nm that can be attributed to π–π* electron transition of 450-CQD sp^2 domains. Figure 14B shows the fluorescence emission spectrum of 550-CQD, The CQD excited at 275 nm UV light show green photoluminescence emission at 480 nm. The excitation dependent emission may be associated with the aromatic C=C bonds and surface defects resulted from C–OH and C=O groups in the 550-CQD [37].

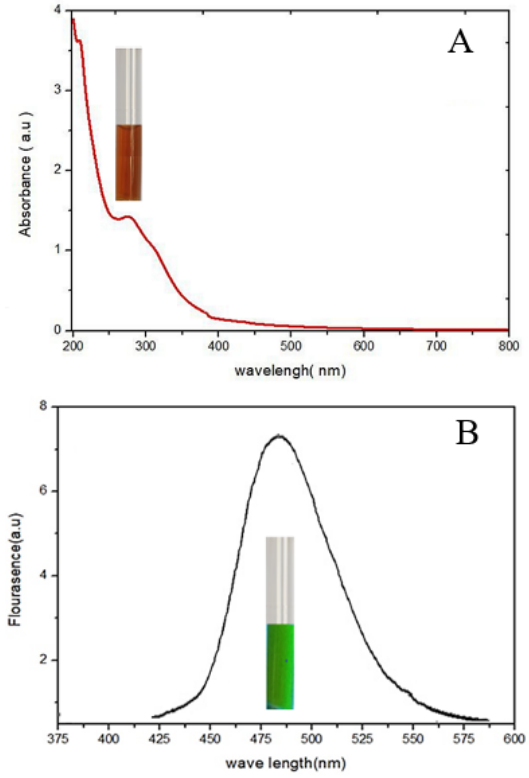

Figure 13. (A) Absorption spectrum of 550-CQD; inset, excitation under UV light and (B) Fluorescence emission; inset, photoluminescence of 550-CQD

The obtained photoluminescence property of 550-CQD reveals it may be useful as an accurate nanotechnology for cancer detection [37] and energy-transfer compound in photocatalytic applications [38,39,40].

4. Conclusion

This study reveals an easy and efficient conversion of a bio-waste material to a valued material. Activated carbon sample with high surface area and proper amount of mesopore volume were synthesized from buffalo dung. The buffalo dung was pre-carbonized char with KOH and pyrolysis at 450°C followed by HCl washing. The obtained activated carbon was modified with metals of Selenium, Bismuth and Zirconium. The electrical parameters of activated carbon and its modified peers were investigated by 4-point probe method. The galvanostatic charge-discharge was also investigated. The electrical testing results displayed that the activated carbon and its metal modification can be used as batteries or capacitor electrodes. Photoluminescence property of activated carbon was also investigated. The results provided promising nanotechnology for cancer detection and energy-transfer in photocatalytic applications.

References

[1] Frackowiak, E., & Béguin, F. "Carbon materials for the electrochemical storage of energy in capacitors". *Carbon*, 39 (6), 937-950, 2001.

[2] Fang, B., Kim, J. H., Kim, M.-S., & Yu, J.-S. "Hierarchical Nanostructured Carbons with Meso–Macroporosity: Design, Characterization, and Applications". *Accounts of Chemical Research*, 46 (7), 1397-1406, 2012.

[3] Candelaria, S.L., Shao,Y., W., Zhou, X. Li, Xiao, J., Zhang, J.-G., Wang, Liu, Y., J., Li, J., & Cao, G. "Nanostructured carbon for energy storage and conversion". *Nano Energy*, 1, 195-220, 2012.

[4] Yang, D.-S., Bhattacharjya, D., Inamdar, S., Park, J., & Yu, J.-S. "Phosphorus-Doped Ordered Mesoporous Carbons with Different Lengths as Efficient Metal-Free Electrocatalysts for Oxygen Reduction Reaction in Alkaline Media". *Journal of the American Chemical Society*, 134 (39), 16127-16130, 2012.

[5] Kim, J. H., Fang, B., Song, M. Y., & Yu, J.-S. "Topological Transformation of Thioether-Bridged Organosilicas into Nanostructured Functional Materials". *Chemistry of Materials*, 24 (12), 2256-2264, 2012.

[6] Yang, D.-S., Bhattacharjya, D., Song, M. Y., & Yu, J.-S. "Highly efficient metal-free phosphorus-doped platelet ordered mesoporous carbon for electrocatalytic oxygen reduction". *Carbon*, 67, 736-743, 2014.

[7] Yang, I., Jung, M., Kim, M.-S., Choi, D., & Jung, J. C. "Physical and chemical activation mechanisms of carbon materials based on the microdomain model". *Journal of Materials Chemistry A*, 9 (15), 9815-9825, 2021.

[8] Li, D., Chen, W., Wu, J., Jia, C. Q., & Jiang, X. "Preparation of waste biomass-derived N-doped carbons and the application in acid gases removal: Focus on N functional groups". *Journal of Materials Chemistry A*, 8, 24977-24995, 2020.

[9] Ying J., Zheng D., Meng S., Yin R., Dai X., Feng J., Wu F, Shi W., & Cao X. "Advanced design strategies for multi-dimensional structured carbon materials for high-performance Zn-air batteries". *New Carbon Mater.* 37 (4), 641-657, 2022.

[10] Wu M., Zhang G., Wang W., Yang H., Rawach D., Chen M., & Sun, S. "Electronic metal-support interaction modulation of single-atom electrocatalysts for rechargeable zinc-air batteries". *Small Methods*, 6 (3), 2100947, 2022.

[11] Lee, J., Kim, J., & Hyeon, T. "Recent Progress in the Synthesis of Porous Carbon Materials". *Advanced Materials*, 18(16), 2073-2094, 2006.

[12] Gumisiriza, R., Hawumba, J. F., Okure, M., & Hensel, O. "Biomass waste-to-energy valorisation technologies: a review case for banana processing in Uganda". *Biotechnology for biofuels*, 10, 1-29, 2017.

[13] Mudasar, R. & Kim, M.H."Experimental study of power generation utilizing human excreta". *Energy Conversion and Management*, *147*, 86-99, 2017.

[14] Plugge, C.M. "Biogas". *Microbial biotechnology*, 10 (5), 1128-1130, 2017.

[15] Jiang, S.F., Sheng, G.P., & Jiang, H. "Advances in the characterization methods of biomass pyrolysis products". *ACS Sustainable Chemistry & Engineering.* 15, 12639-12655, 2019.

[16] Xu, X., Ray, R., Gu, Y., Ploehn, H. J., Gearheart, L., Raker, K., & Scrivens, W. A. "Electrophoretic Analysis and Purification of Fluorescent Single-Walled Carbon Nanotube Fragments". *Journal of the American Chemical Society*, 126 (40), 12736-12737, 2004.

[17] Kim, S., Hwang, S. W., Kim, M.-K., Shin, D. Y., Shin, D. H., Kim, C. O., … & Hong, B. H. "Anomalous Behaviors of Visible Luminescence from Graphene Quantum Dots: Interplay between Size and Shape". *ACS Nano*, 6(9), 8203-8208, 2012.

[18] Li, L., Wu, G., Yang, G., Peng, J., Zhao, J., & Zhu, J.J. "Focusing on luminescent graphene quantum dots: current status and future perspectives". *Nanoscale*, 5(10), 4015-39, 2013.

[19] Liu, W.W., Feng, Y.Q., Yan, X.-B., Chen, J. T., & Xue, Q.J. "Superior Micro-Supercapacitors Based on Graphene Quantum Dots". *Advanced Functional Materials*, 23 (33), 4111-4122, 2013.

[20] Liu, F., Jang, M. H., Ha, H. D., Kim, J. H., Cho, Y. H., & Seo, T. S. Facile Synthetic Method for Pristine Graphene Quantum Dots and Graphene Oxide Quantum Dots: Origin of Blue and Green Luminescence. *Advanced Materials*, 25 (27), 3657-3662, 2013.

[21] Lu, J., Yeo, P.S.E., Gan, C.K., Wu, P., & Loh, K.P. "Transforming C60 molecules into graphene quantum dots". *Nat Nanotechnol*, 6(4), 247-252, 2011.

[22] Peng, J., Gao, W., Gupta, B. K., Liu, Z., Romero-Aburto, R., Ge, L., … & Ajayan, P. M. Graphene Quantum Dots Derived from Carbon Fibers. *Nano Letters*, 12(2), 844-849, 2012.

[23] Xu, J., Zhou, Y., Liu, S., Dong, M., & Huang, C. "Low-cost synthesis of carbon nanodots from natural products as fluorescent probe for the detection of ferrum (III) ion in lake water". *Anal Methods*, 6(7), 2086-2090, 2014.

[24] Liang, Q., Ma, W., Shi, Y., Li, Z., & Yang, X. "Easy synthesis of highly fluorescent carbon quantum dots from gelatin and their luminescent properties and applications". *Carbon*, 60, 421-428, 2013.

[25] Sun, D., Ban, R., Zhang, P.H., Wu, G.H., Zhang, J.R., & Zhu, J.J. "Hair fiber as a precursor for synthesizing of sulfur-and nitrogen-co-doped carbon dots with tunable luminescence properties". *Carbon*, 64, 424-434, 2013.

[26] Lu, Y., Shan, G., Huang, J., & Li, Q. "Insights into characteristics of dissolved organic matter fractions in co-composted dairy manure and Chinese herbal residues". *Waste Biomass valorization*, 9, 777-782, 2018.

[27] Cantrell, K.B., Ducey, T., Ro, K.S., & Hunt, P.G. "Livestock waste-to-bioenergy generation opportunities". *bioresource technology*, 99, 7941-7953, 2008.

[28] Chen, Z.L., Zhang, J.Q., Huang, L., Yuan, Z.H., Li, Z.J., & Liu, M.C. "Removal of Cd and Pb with biochar made from dairy manure at low temperature". *Journal of Integrative Agriculture*, 18, 201-210. 2019.

[29] Tsai, T.W., Hsu, C.H., & Lin, Y.Q. "Highly porous and nutrients-rich biochar derived from dairy cattle manure and its potential for removal of cationic compound from water". *Agriculture*, 9, 114, 2019.

[30] Cao, H.L., Xin, Y., & Yuan, Q.X. "Prediction of biochar yield from cattle manure pyrolysis via least squares support vector machine intelligent approach". *bioresource technology*, 202, 158-164, 2016.

[31] Miao, M., Zuo, S., Zhao, Y., Wang, Y., Xia, H., Tan, C., & Gao, H. "Selective oxidation rapidly decomposes biomass-based activated carbons into graphite-like crystallites". *Carbon*, 140, 504, 2018.

[32] Alabadi, A., Razzaque, S., Yang, Y., Chen, S., & Tan, B. "Highly porous activated carbon materials from carbonized biomass with high CO_2 capturing capacity", *chemical engineering journal*, 281, 606-612, 2015.

[33] Luo, L., Chen, T., Li, Z., Zhang, Z., Zhao, W., & Fan, M. "Heteroatom self-doped activated biocarbons from fir bark and their excellent performance for carbon dioxide adsorption". *Journal of CO2 Utilization*, 25, 89-98, 2018.

[34] Bae, J., & Su, S. "International Journal of Greenhouse Gas Control Macadamia nut shell-derived carbon composites for post combustion CO 2 capture". *International journal of greenhouse gas control*, 19, 174-182, 2013.

[35] Chen, C., Zhao, P., Huang, Y., Tong, Z., & Li, Z. "Preparation and characterization of activated carbon from Eucalyptus sawdust I. Activated by NaOH". *Journal of Inorganic and Organometallic Polymers and Materials*, 23, 1201-1209, 2013.

[36] Farma, R., Deraman, M., Awitdrus, I. A., Tahlib, E., Taer, N. H., Basri, J. G., Manjhunata, M. M., Isbak, B. N. M., & Hashmi, S. A. "Preparation of Highly Porous Binderless Activated Carbon Electrodes from Fibres of Oil Palm Empty fruit Bunchess for Application in Supercapasitor". *Biresource Technology*, 132, 254-261, 2013.

[37] Ramos-Ramón, J.A., Bogireddy, N.K.R., Giles Vieyra, J.A., Karthik, T.V.K. & Agarwal, V. "Nitrogen-Doped Carbon Dots Induced Enhancement in CO2 Sensing Response From ZnO–Porous Silicon Hybrid Structure". *Frontiers in Chemistry*, 8, 291, 2020.

[38] Lu, W., Qin, X., Liu, S., Chang, G., Zhang, Y., Luo, Y., Asiri, A., Al-Youbi, A., & Sun, X. "Economical, green synthesis of fluorescent carbon nanoparticles and their use as probes for sensitive and selective detection of mercury(II) ions". Analytical Chemistry, 84, 5351-5357, 2012.

[39] Liu, S., Tian, J., Wang, L., Zhang, Y., Qin, X., Luo, Y., Asiri, A. M., Al-Youbi, A. O., & Sun, X. "Hydrothermal treatment of grass: A low cost, green route to nitrogen-doped, carbon-rich, photoluminescent polymer nanodots that can be used as an effective fluorescent sensing platform for label-free sensitive and selective detection of Cu(II) ions". *Advanced Materials*, 24, 2307-2310, 2012.

[40] Zhang, H., Huang, H., Ming, H., Li, H., Zhang, L., Liu, Y., & Kang, Z. "Carbon quantum dots/Ag3PO4 complex photocatalysts with enhanced photocatalytic activity and stability under visible light". *Journal of Materials Chemistry*, 22, 10501-10506, 2012.